Research Article | Vol. 12, No. 2 / 1 February 2021 / Biomedical Optics Express 836

Biomedical Optics EXPRESS

Optical diagnosis of oral cavity lesions by label-free Raman spectroscopy

LEVI MATTHIES,[1,6,*] MEDHANIE T. GEBREKIDAN,[2,3,6] JASPER F. TEGTMEYER,[1] NICOLAI OETTER,[2,4] MAXIMILIAN ROHDE,[4] TOBIAS VOLLKOMMER,[1] RALF SMEETS,[1] WALDEMAR WILCZAK,[5] FLORIAN STELZLE,[2,4] MARTIN GOSAU,[1] ANDREAS S. BRAEUER,[3] AND CHRISTIAN KNIPFER[1]

[1] *University Medical Center Hamburg-Eppendorf (UKE), Department of Oral and Maxillofacial Surgery, Martinistraße 52, D-20246 Hamburg, Germany*
[2] *Friedrich-Alexander-Universität Erlangen-Nürnberg (FAU), Erlangen Graduate School in Advanced Optical Technologies (SAOT), Paul-Gordan-Straße 6, D-91054 Erlangen, Germany*
[3] *Technische Universität Bergakademie Freiberg (TUBAF), Institute of Thermal-, Environmental- and Resources' Process Engineering (ITUN), Leipziger Straße 28, D-09599 Freiberg, Germany*
[4] *Friedrich-Alexander-Universität Erlangen-Nürnberg (FAU), Department of Oral and Maxillofacial Surgery, Glückstraße 11, D-91054 Erlangen, Germany*
[5] *University Medical Center Hamburg-Eppendorf (UKE), Institute of Pathology, Martinistraße 52, D-20246 Hamburg, Germany*
[6] *These authors contributed equally*
[*] *l.matthies@uke.de*

Abstract: Oral squamous cell carcinoma (OSCC) is one of the most prevalent cancers and frequently preceded by non-malignant lesions. Using Shifted-Excitation Raman Difference Spectroscopy (SERDS), principal component and linear discriminant analysis in native tissue specimens, 9500 raw Raman spectra of OSCC, 4300 of non-malignant lesions and 4200 of physiological mucosa were evaluated. Non-malignant lesions were distinguished from physiological mucosa with a classification accuracy of 95.3% (95.4% sensitivity, 95.2% specificity, area under the curve (AUC) 0.99). Discriminating OSCC from non-malignant lesions showed an accuracy of 88.4% (93.7% sensitivity, 76.7% specificity, AUC 0.93). OSCC was identified against physiological mucosa with an accuracy of 89.8% (93.7% sensitivity, 81.0% specificity, AUC 0.90). These findings underline the potential of SERDS for the diagnosis of oral cavity lesions.

© 2021 Optical Society of America under the terms of the OSA Open Access Publishing Agreement

1. Introduction

Oral cavity squamous cell carcinoma (OSCC) is among the most common cancers worldwide, predominantly in men [1–3]. Over 350,000 new incident cases and 150,000 deaths were reported in 2018 [2]. Despite advances in the therapeutic regimen, the 5-year survival rate for OSCC patients has remained around 50% over the last 50 years [1]. One of the main reasons is that the curability of cancer generally depends on the stage at discovery, and although the oral cavity is easily accessible, most OSCC are diagnosed at an advanced stage (UICC III and IV) [4]. Anatomic disease extent according to the Union for International Cancer Control (UICC) TNM classification, i.e. stage, is the major determinant of appropriate treatment and prognosis [5]. Herein, the T category describes primary tumor site, N describes regional lymph node involvement and M describes distant metastatic spread. Moreover, patients with OSCC have an increased chance of developing recurrence or a second primary tumor. This depends on a variety of factors, such as histopathological tumor grading, TNM classification including surgical margin status, continued exposure to carcinogens, or occult replacement of the normal

#409456 https://doi.org/10.1364/BOE.409456
Journal © 2021 Received 7 Sep 2020; revised 21 Nov 2020; accepted 8 Dec 2020; published 13 Jan 2021

Biomedical Optics EXPRESS

cell population by a cancer-primed cell population that may initially display no morphological change, a phenomenon called "field cancerization" [6–8]. Early diagnosis of OSCC (UICC stage I and stage II) however, can lead to improved curing rates of above 90% [9]. According to current guidelines for the diagnosis and treatment of oral cavity carcinoma, conspicuous, irregular mucosal areas require an initial monitoring and conservative treatment. In case of persistence, the current gold standard to establish a diagnosis and detect potential malignancy is the histopathological analysis after surgical excision [10–12]. Adhering to the WHO Classification of Head and Neck Tumors 4th edition, OSCC is the principal malignant surface epithelial tumor of the oral cavity and mobile tongue [13,14]. Accordingly, OSCC may be preceded by oral potentially malignant disorders (OPMD), initially benign lesions, associated with a statistically increased risk of developing oral cancer, such as forms of leukoplakia or erythroplakia [8,15]. Herein, histological grading of epithelial dysplasia as mild, moderate or severe by an evaluation of cytological and architectural changes, determines potential malignant transformation [16]. Among OPMD, the subgroup of proliferative verrucous leukoplakia with severe dysplasia shows probability of malignant transformation of up to 50% [17]. In erythroplakia, histologically severe dysplasia or even carcinoma in situ is frequently observed [18]. Furthermore, abnormal DNA content, overexpression of molecular tumor markers such as p53 or Cyclin D1 underline the potential for malignant transformation of over 30% [17,19]. Therefore, surgical excision with safety margins is indicated. In inflammation or ulceration, tissue destruction or bleeding may be characteristic, similar to oral cancer. Other lesions such as irritant fibroma or hyper-/parakeratosis show little to no potential for malignant transformation [17]. As the clinical aspects often overlap, the distinction can be challenging, even to experienced practitioners and sometimes extensive monitoring and/or follow-up biopsies are required. For patients this may invoke fear, stress, pain and iatrogenic damage to healthy tissue. Ascertaining the histopathological diagnosis determines the subsequent treatment options, thus needs to be performed thoroughly and therefore requires time [17]. Ultimately, results also depend on quality of the surgical sample and pathological expertise. At this point in the diagnostic pathway, there is an unmet need for immediate objective identification of OSCC against non-malignant mucosal lesions at an early stage. To reduce uncertainties in the diagnostic gap between clinical examination and histopathological analysis, the development of a non-invasive method capable of discriminating an OSCC from conspicuous, non-malignant conditions in real time, with a minimal misclassification rate, is desirable.

The implication of optical technologies for early diagnosis of OSCC and premalignant stages is a field of research in constant progress [20]. It has involved fluorescence spectroscopy [21,22], Raman spectroscopy [23–27], and confocal laser endomicroscopy [28–30]. The optical characterization of molecular tissue constituents has great potential for cancer diagnostics and therapeutic options [31,32]. The Raman spectrum contains information about the molecular composition of biological tissue, such as the content of lipids, nucleic acids, proteins and water, from which its patho-physiological status can be retrieved. Specific biomolecules, for example keratin, an epithelial cellular structural protein, are aberrantly expressed in tumors, which can be used as inherent and naturally occurring cancer molecular indicators [33]. Raman spectroscopy, coupled with multivariate analysis, has been shown to be capable of identifying esophageal, prostate, uterine and cervical cancer tissue [34]. Oral cancers, and other tumor entities, are often derived from precancerous conditions, that exhibit specific changes in their cellular and biochemical composition [35]. Hence, the aim of the present study was to investigate whether Raman spectroscopy has the potential to discriminate conspicuous lesions of the oral cavity.

In the present study, the discrimination of physiological mucosa, non-malignant lesions and OSCC using Shifted-Excitation Raman Difference Spectroscopy (SERDS) was evaluated. This technique was first proposed by Shreve et al. and has been established as a useful tool for applying Raman spectroscopy to samples with strong fluorescence interference, such as viable biologic tissues [36–39]. Kasha discovered that the fluorescence signal is nearly insensitive to small

Biomedical Optics EXPRESS

photon energy excitation changes in contrast to the Raman spectrum which shifts according to the excitation photon energy difference [40]. Thus, subtracting two raw spectra, each excited with a slightly different photon energy, enables the elimination of the fluorescence background, while a Raman difference spectrum remains. The SERDS efficiently eliminates both, fluorescence interference and systematic background, such as etaloning, from spectra without any kind of sample preparation [41,42]. The major advantage of the SERDS technique is that the fluorescence is eliminated mainly because of a physical approach. Thus, in contrast to purely mathematical based baseline correction approaches, it does not affect the Raman features of the spectrum [43]. To the best of our knowledge, this is the first report using SERDS for the investigation of malignant and non-malignant lesions of the oral cavity.

2. Method

2.1. Sample preparation

For this study, a total of 37 patients were enrolled from the Department of Oral and Maxillofacial Surgery, University Medical Center Hamburg-Eppendorf, Germany. Raman spectra were collected from biopsy samples of clinically apparent, conspicuous lesions (n=22), as well as from the central aspect of histo-pathologically confirmed bulk OSCC resectates (n=15) and the corresponding surgical safety margins (i.e. healthy, physiological mucosa, n=9). The former were taken under local anesthesia in the outpatient clinic, whereas the latter were obtained under general anesthesia in the operating room. Anatomic locations of the oral cavity were as follows: hard/soft palate, alveolar ridge, floor of the mouth, tongue, cheek, inner lip. Label-free tissue specimens were stored in their native state (isotonic 0.9% NaCl solution). According to clinical workflow and feasibility, the samples were either processed for spectroscopic analysis immediately, or temporarily stored at 4 °C for a maximum period of six hours. To reduce the effect of background interference, a dark Teflon sheet was used as a base (see Fig. 1(A)). For each biopsy sample, after anatomical orientation, in average three measurement locations were chosen on the mucosal aspect. These laser focal spots were equally distributed over the sample with a minimum distance of 2 mm in between. In 9 out of 15 resected bulk tissue specimens, OSCC was centrally located. Currently, there is no uniformity in the definitions of adequate surgical margins. In a survey of the American Head and Neck Society, members were asked how they evaluate and define tumor margins [44]. The most common response for distance of a clear pathologic margin was >5 mm on microscopic evaluation, which is in accordance with the guidelines of the Royal College of Pathologists [45]. This definition was adopted and followed by the authors. Histopathologically verified oncologic resection safety margins of 5 mm healthy, normal tissue were utilized as reference for peripheral measurements of physiological mucosa. If the histopathological findings revealed marginal resection, distance of < 5 mm or a dysplastic front, clinically an extension of the surgical margins was performed, and samples were not proceeded for optical measurements. With regards to heterogeneity of the sample, including muscle, adipose tissue, bone or salivary gland tissue, only the mucosal aspects of the specimens were analyzed. In consultation with the attending surgeon, the bulk tissue specimens were assessed and marked with colored needles indicating anatomical orientation. From each of these samples, in average eight evenly distributed measurement locations (four central and four peripheral), with a minimum distance of 2 mm in between, were chosen. The difference in the number of measurement locations between the biopsies and resected samples was due to the size of the samples. The typical dimensions of biopsies were smaller than 1×1x1 cm^3, whereas resected samples exceeded this and often amounted to 5×5x5 cm^3 and more. After optical measurements, specimens were evaluated by the Institute of Pathology as part of the clinical routine. Following histopathological confirmation, spectroscopic data was referenced with the according entities.

Biomedical Optics EXPRESS

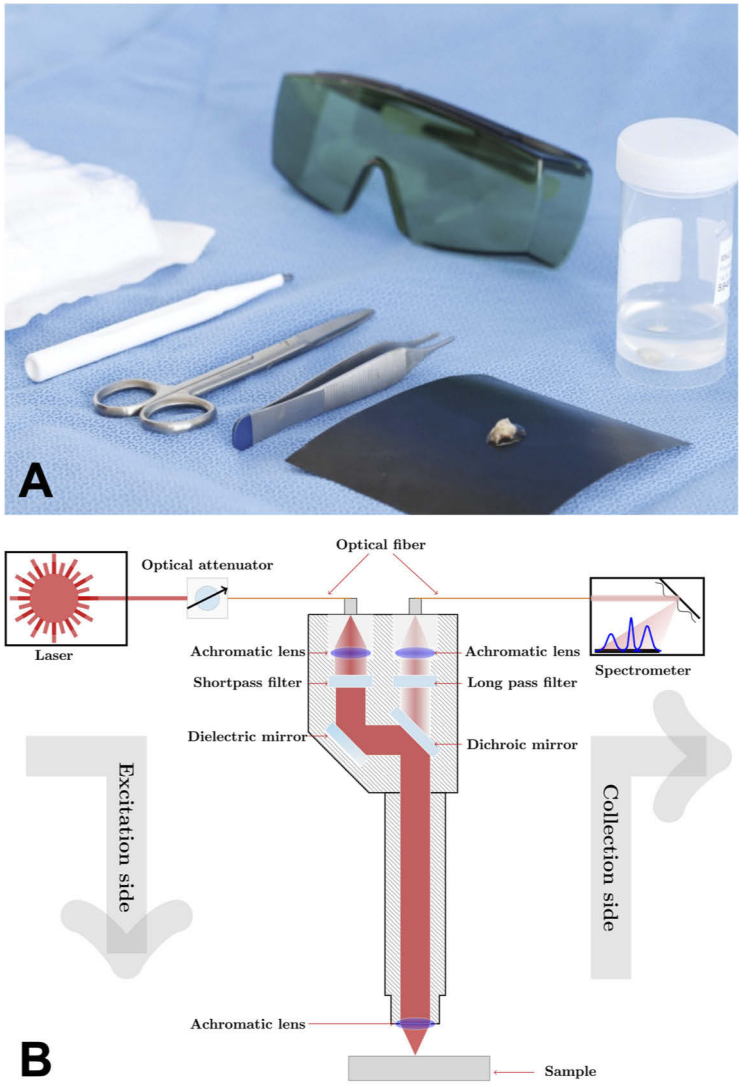

Fig. 1. Experimental Setup. (A) Tissue specimen stored in NaCl solution, prepared for analysis on Teflon sheet. (B) Schematic figure of self-engineered, compact and portable Raman sensor consisting of a tunable diode laser, a fiber coupled spectrometer and Raman probe.

Biomedical Optics EXPRESS

2.2. Technical Setup

For the utilization of Raman spectroscopy in this study design, a Raman sensor was self-developed (see Fig. 1(B)) [43]. A diode laser (DLpro, Toptica photonics, Munich, Germany) with a variable wavelength tunable between 770 and 810 nm and a linewidth of less than 500 kHz is used as the excitation light source. The laser power of 1 W is attenuated to 115 mW using a Glan-laser prism combined with a half-wave plate. The excitation beam is launched into a glass fiber (200 µm core diameter, 0.22 NA, Ocean Optics, Rochester, New York, USA), which guides the laser radiation to a Raman probe. Inside the Raman probe, a short pass filter (780/12 Brightline HC, Semrock, Rochester, New York, USA) suppresses wavelengths longer than 785 nm originating from fiber-light interactions when the excitation light passes through the glass fiber. The excitation laser beam is then reflected via a dichroic mirror, which is highly reflective for the excitation wavelength but transparent for wavelengths longer than 785 nm. It is then focused through a lens (achromatic lens, THORLABS, Newton, New Jersey, USA) onto the sample with a focal spot diameter of approximately 200 µm and axial resolution of approximately 5 µm. The axial resolution was estimated mathematically.

$$\text{axial resolution} \approx \frac{\lambda}{\text{NA}^2},\ \lambda = 785\text{nm}, \text{Numerical Aperture (NA)} \approx 0.4 \tag{1}$$

A portion of the excited signals (these are mainly elastic light scattering signals, fluorescence and the desired Raman signals) is detected in back-scattering direction through the same lens. The red-shifted fluorescence and Raman signals pass the dichroic mirror towards another lens focusing them onto a detection glass fiber (600 µm core diameter, 0.37 NA, Ocean Optics, Rochester, New York, USA) guiding the signals from the Raman probe to the spectrometer (Ventana-785-Raman, Ocean Optics, Rochester, New York, USA). The elastic light scattering signals are filtered out, first, by the dichroic mirror reflecting them towards the excitation glass fiber and, second, by a long pass filter mounted between the dichroic mirror and the signal focusing lens. The Ventana spectrometer analyzes the spectra between 800 and 940 nm, which corresponds to Raman shifts from 200 to 2000cm^{-1}. The spectral resolution is specified at 810 nm to be 10 cm^{-1}. At 810 nm, a wavenumber difference of 10 cm^{-1} corresponds to approximately 0.6 nm. Therefore, signals with a wavelength difference of minimum 0.6 nm can be spectrally resolved as two different peaks. With 1024 pixels along the spectral axis of the detector, one pixel corresponds to approximately 0.137 nm (~2.44 cm^{-1}), which is below the spectral resolution.

Three combined and electrically driven linear translation stages (NRT150, THORLABS, Newton, New Jersey, USA) were used to move the handheld Raman probe to selected points on the sample in the xyz-space. The 3D coordinates of a selected measurement point on the sample were provided by a 3D visualization system (Ensenso N10 stereo camera, IDS Imaging Development Systems, Obersulm, Germany). The focal spot position was optimized for maximum signal intensity through the z-translation stage in every measurement point, being focused on the epithelial surface. As the laser beam penetrates the tissue, the optical density of the focal spot decreases due to scattering and absorption processes, thus the Raman signal is expected to originate predominantly from the epithelium [46]. This combination of translation stages and 3D camera made the subsequent detection of Raman spectra from different measurement locations on the tissue sample efficient.

2.3. Analysis

At each of the identified measurement locations, 50 single spectra were acquired using the excitation wavelength of 784 nm. For the acquisition of one spectrum, the integration time, was set to 1 second (1000 ms). Then the excitation wavelength was automatically shifted to 785 nm, and another 50 single spectra were recorded from the same measurement location. Mean spectra were averaged from each of the 50 raw spectra. The extraction of pure Raman spectra from the

Biomedical Optics EXPRESS

heavily autofluorescence interfered raw mean spectra was done according to the SERDS method previously described by our workgroup in detail [43] and in short in the following: the two mean raw spectra, one for each excitation wavelength (784 and 785 nm), are first z-score normalized to bring them into the same scale. Then the normalized spectra are subtracted from each other to get a Raman-difference spectrum. As the fluorescence background is supposed to not be influenced by the excitation wavelength, the majority of the fluorescence background is eliminated by the subtraction. However, due to photo-bleaching, the resulting difference spectrum still contains fluorescence residuals. The residual fluorescence, already vastly reduced compared to the original fluorescence level, is eliminated further using mathematical approaches. First, the center of the difference spectrum is identified using an asymmetric least squares fit and subtracted from the difference spectrum. Then a spectrum is reconstructed from the center-corrected difference spectrum using a mathematical recurrence relation. The obtained reconstructed spectrum still contains a weak fluorescence background which is eliminated further by applying a baseline correction based on piecewise asymmetric least squares fitting. Finally, a pure reconstructed Raman spectrum is obtained.

In order to differentiate between physiological mucosa, OSCC and non-malignant lesions, Raman shifts between 630 to 1800cm^{-1} were considered. These spectra were first vector normalized for principal component analysis (PCA). PCA is a preprocessing method to reduce the number of spectral parameters by generating a new set of independent features ordered by the largest variability in the dataset [47]. After that, the differentiation performance between OSCC and physiological mucosa, OSCC and non-malignant lesions, physiological mucosa and non-malignant lesions was investigated. To this end, three separate classification models based on linear discriminant analysis (LDA) were made [48]. Each model was tested by implementing 5-fold cross validation which divided the spectral dataset into training and test datasets in an iterative loop. In each cross-validation iteration, ~80% of the dataset were used to train the model and ~20% of the dataset were used to test its predication capability. A nested inner cross-validation was also implemented to compute the optimal number of principal components and hyperparameters of the classifier based on sequential model-based optimization (also known as Bayesian optimization) [49]. Moreover, in order to avoid introducing bias to the disadvantage of classes with minority datasets, each classifier received an equal distribution of both classes for training by applying methods to deal with data imbalance [50].

3. Results

In total, 42 Raman spectra of healthy, physiological mucosa, 95 Raman spectra of OSCC and 43 Raman spectra of non-malignant lesions were collected from biopsies and resected bulk tissue samples. Altogether, 22 clinically apparent, conspicuous mucosal lesions, not regressing upon monitoring and conservative treatment, therefore warranting surgical biopsy, included one physiological mucosa sample, seven oral squamous cell carcinoma (OSCC) and 14 non-malignant lesions. The non-malignant lesions involved distinct histopathological entities such as inflammation, leukoplakia, dysplasia, hyperkeratosis and irritant fibroma. In this pilot study these lesions were grouped as non-malignant at this point. Table 1 summarizes the analyzed tissues.

Table 1. Summary of patient data and tissue types used in this report

Tissue form	Biopsy		Resected OSCC		Total		
	Samples	Meas. locations	Samples	Meas. locations	Samples	Meas. locations	Sites
Physiological mucosa	1	3	9	39	10	42	8
OSCC	7	23	15	72	22	95	9
Non-malignant lesions	14	43			14	43	8

Biomedical Optics EXPRESS

Figure 2 shows the mean SERDS reconstructed Raman spectra of physiological tissue (green line), OSCC (red line) and non-malignant lesions (black line) that were averaged from 42, 95 and 43 reconstructed Raman spectra, respectively. Annotations assign the spectral Raman signatures to their known molecular origin. The differences between physiological and pathological tissues (non-malignant and OSCC) are noticeable in the whole spectral region analyzed, although more pronounced in the fingerprint region (1200–1800cm^{-1}). The differences between malignant and non-malignant lesions were less pronounced and occurred mainly in the region between 800 to 1400 cm^{-1}. The spectral features of physiological tissue of the oral cavity reflected dominant contribution from lipid molecules, a strong CH_2 band around 1448 cm^{-1}, two sharp peaks/bands around the amide III region, a sharper peak around the amide I region and altered nucleic acid spectral features. In contrast, spectra from non-malignant and OSCC tissues feature broader amide I and III regions, a shifted and weaker CH_2 band and a strong phenylalanine peak.

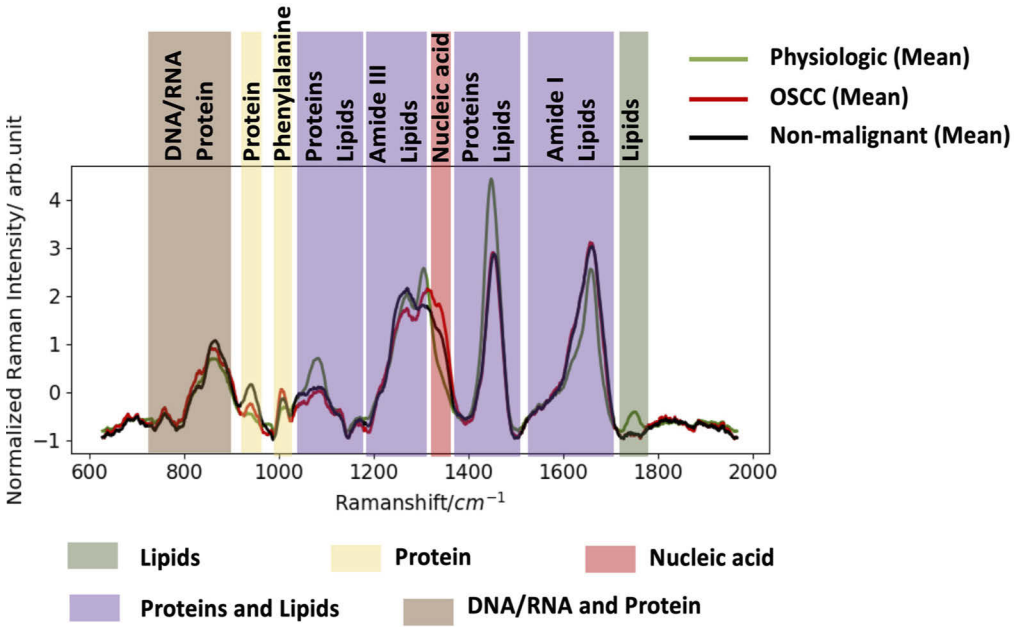

Fig. 2. Reconstructed mean Raman spectra of physiological oral tissue (green line), malignant (red) and non-malignant lesions (black) and with peak position assignment to their respective molecular origin. Lipids (light green), protein (light yellow), both proteins and lipids (light magenta), nucleic acid (light red), and proteins, nucleic acid and carbohydrates (light brown).

Looking at the mean Raman spectra in Fig. 2, several spectral features can be selected to differentiate physiological tissue from conspicuous lesions, irrespective of whether the diseased tissue is classified as non-malignant or OSCC. Vibration of the C = O lipid band at 1750cm^{-1} can be considered as one criterion for differentiation because it only exists in the physiological tissue. The physiological mucosa spectral peak/band at 1656 cm^{-1} in the amide I region, resulting from the C = C lipid band, is sharper than the amide I peak of the diseased tissue at around 1660 cm^{-1}. The CH_2 band of proteins at around 1451 cm^{-1} in the diseased tissue also appears shifted from and weaker in intensity than the equivalent band of lipids in the physiological tissue. The phenylalanine spectral feature around 1003 cm^{-1} is stronger in the diseased tissue as compared to the physiological tissue. Overall, the differences between malignant and non-malignant lesions are less pronounced.

Biomedical Optics EXPRESS

In Fig. 3, the difference spectrum (mean spectrum of OSCC minus mean spectrum of non-malignant lesions) shows the major spectral differences between the diseased tissues. Larger differences were noticed due to varying nucleic acid content and changes associated to the amide III region. The differences around the amide I region and due to the CH_2 band are minimal.

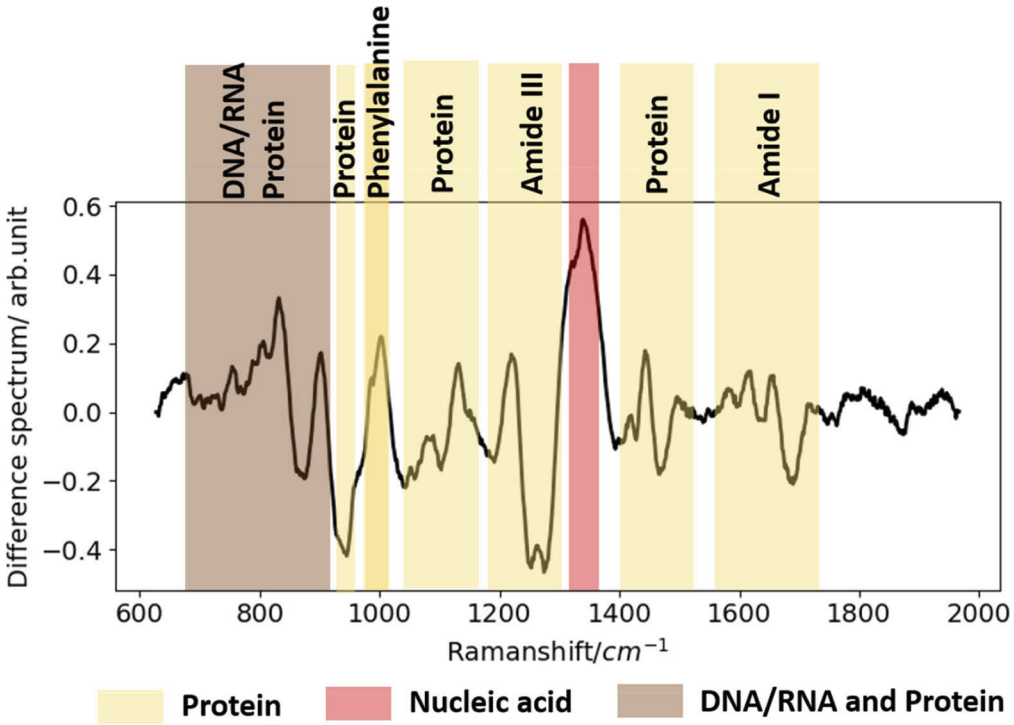

Fig. 3. Difference spectrum of mean Raman spectrum of non-malignant lesions subtracted from mean Raman spectrum of OSCC with difference peak assignments to their respective molecular origin, protein (light yellow), nucleic acid (light red), and both proteins and nucleic acid (light brown).

In Fig. 4, the result of the principal component analysis between 43 measurements of non-malignant lesions (hyperkeratosis, inflammation, irritant fibroma, leukoplakia and dysplasia), 95 of OSCC and 42 of physiological mucosa are shown. In this presentation, the distinct tissue categories are grouped according to the first three principal components (PC1, PC2, PC3) and separable with little overlap. In this dataset, the first principal component contains 45.08% of the spectral variation of the oral tissues. The second principal component accounts for 19.96%, the third comprises 9.50%. The fourth and fifth principal components amount to 12.57% of spectral variation.

To elucidate the aspects of differentiation, the principal component loading plots can be seen in Fig. 5. Herein, the correlation between the principal components and Raman spectral contribution are indicated in shaded black color. Black shows higher contribution of the Raman peaks/bands to the respective principal component. The main contribution to the first principal component are the CH_2 band of lipid (1448 cm^{-1}), the CH_2 band of protein (1451 cm^{-1}), C-H bending mode of structure protein (1453 cm^{-1}), C-C or C-O stretch (1078 cm^{-1}), C = C stretch or tryptophan at 1618 cm^{-1}, amide III and nucleic acid at 1340 cm^{-1}. The second principal component contains spectral variation related to the amide I region, nucleic acid (1340 cm^{-1}), amide III, phenylalanine at 1002/3 cm^{-1} and proline (943 cm^{-1}). The contribution to the third principal components are assignable to proline (855 cm^{-1}), O-P-O stretch DNA/RNA (828 cm^{-1}), lipid/C-C stretching

Biomedical Optics EXPRESS

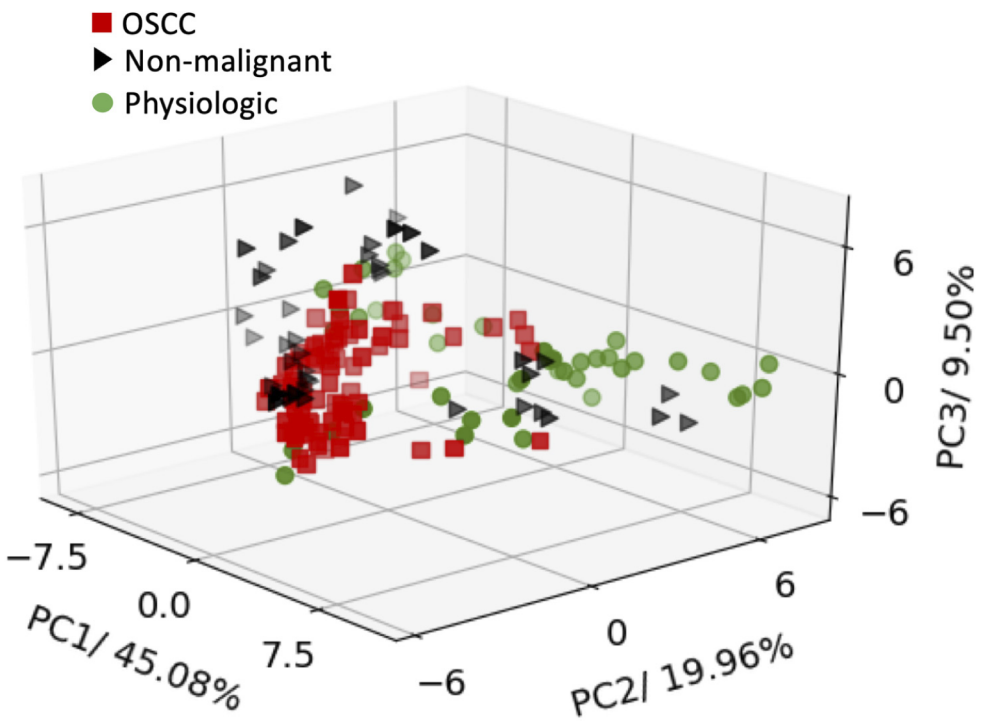

Fig. 4. Principal Component Analysis scores of Raman spectra of OSCC (red squares), non-malignant lesions (black triangles) and physiological mucosa (green circles) collected from 180 measurements.

(collagen) at 868 cm^{-1} and CH_2 twisting of lipid at 1301 cm^{-1}. The fourth and fifth principal components are mainly assignable to amide III, nucleic acid (1340 cm^{-1}) and proline (1043 cm^{-1}). These PC loadings demonstrate that the differentiation between OSCC, non-malignant lesions and physiological mucosa is sensitive to and determined by the biochemical composition of the tissue.

The feasibility of the classification of physiological, non-malignant and malignant lesions was explored using LDA. Three LDA classification models were set up to distinguish between three different datasets: physiological mucosa vs. non-malignant lesions, physiological mucosa vs. OSCC, and non-malignant lesions vs. OSCC. Figure 6 illustrates the receiver-operating characteristic curve (ROC) that visualizes the performance of the three classifiers. In the physiological mucosa vs. non-malignant lesions classification, we found a 5-fold cross-validation accuracy of 95.3% at a sensitivity of 95.4% and specificity of 95.2%. The area under the curve was found to be 0.99, with only four out of 85 tissue spectra being misclassified. Spectral classification of OSCC against physiological mucosa gave an overall accuracy of 89.8% at a sensitivity of 93.7% and specificity of 81.0%. Here, a total of 123 out of 137 were correctly classified while eight physiological tissue samples were falsely classified as OSCC and six OSCC were misclassified as physiological tissue. The respective AUC was determined to be 0.90. Classification of OSCC against non-malignant tissues resulted in a sensitivity of 93.7% and specificity of 76.7%. In total, 122 out of 138 pathological tissues were correctly classified while 16 were falsely classified giving an overall accuracy of 88.4% and an AUC of 0.93.

Biomedical Optics EXPRESS

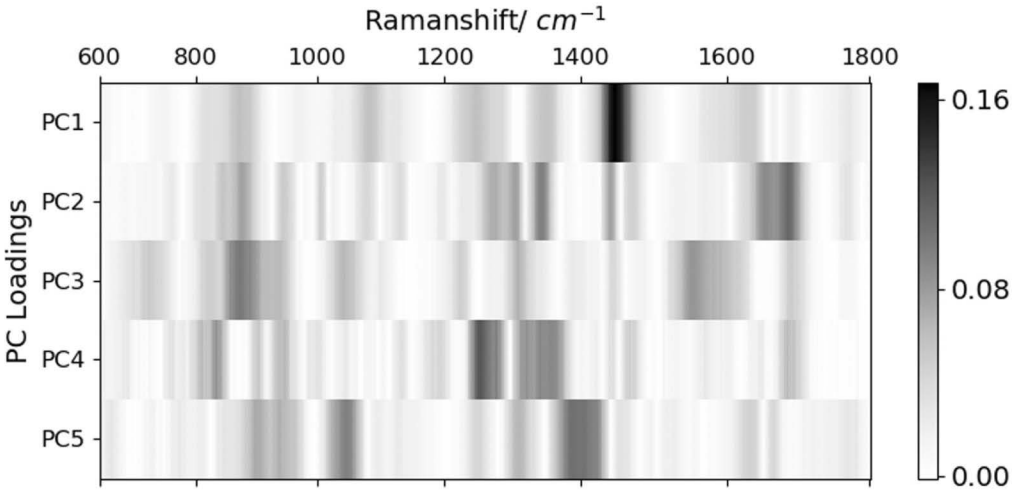

Fig. 5. PC loading plot for the first five principal components as a function of the Raman shift.

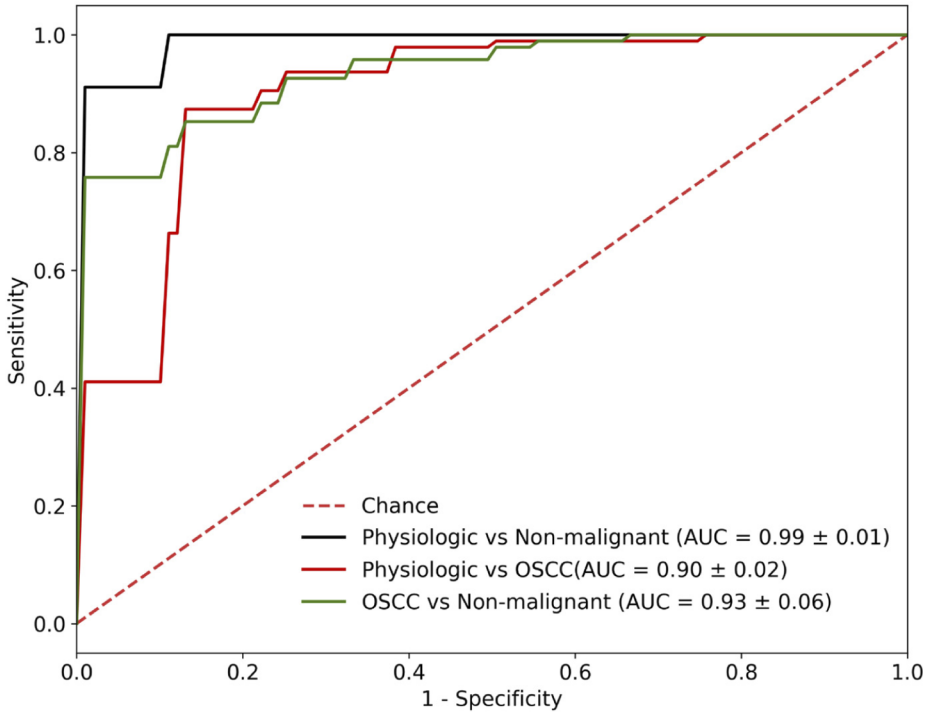

Fig. 6. Receiver-operating characteristic curve. Performance of the PCA-LDA classifiers, between physiological mucosa and non-malignant lesions (black curve), physiologic vs. OSCC (red curve), and OSCC against non-malignant lesions (green curve).

Biomedical Optics EXPRESS

4. Discussion

The characterization of molecular tissue content by Raman spectroscopy has great potential for oral cancer diagnostics and is constantly progressing [34]. Our findings demonstrate distinction of conspicuous, non-malignant lesions, that warranted confirmation by surgical biopsy, from OSCC and physiological mucosa. The method is based on non-invasive Raman spectroscopy in combination with PCA-LDA analysis and classification. The data indicate that the majority of the spectral features of malignant and non-malignant lesions of the oral cavity originate from protein and nucleic acid molecules. With regards to the available literature, spectroscopic features around 1750cm^{-1}, 1660 cm^{-1}, 1451 cm^{-1} or 1003 cm^{-1} were particularly pronounced in our experimental setup and therefore useful for distinction [51–57]. This reflects that with the severity of pathological properties and malignant transformation in oral cancer, protein-related features [58] and DNA increase [58,59] while lipid features decrease [60–62]. This change from lipid to protein and DNA in accordance with pathological changes may be attributed to changes in tissue architecture and morphology, increased angiogenesis and cellular proliferation in premalignant and malignant conditions [58].

There is a wide variety of Raman spectroscopy methods and applications in biomedical research in general and in oral cancer diagnostics in particular [34]. Li et al. applied Fourier transformation near infrared (FT-NIR) Raman spectroscopy to differentiate between normal, OSCC and dysplastic tissues at different stages [63]. Compared to physiological mucosa, the authors observed high contents of protein and DNA in oral dysplasia and OSCC. Another approach in oral cancer diagnosis via Raman spectroscopy is the analysis of specific biomolecules. Keratin is a structural protein protecting epithelial cells from damage. It can be considered a molecular indicator for some entities of epithelial cancers, such as oral squamous cell carcinoma. Chen et al. analyzed OSCC tissues by spectral matching comparison of decomposed Raman spectra and the standard Raman spectrum of keratin [64]. The decomposed spectral components in the OSCC tissue samples had higher similarity with the standard keratin spectrum than those in the normal tissue. For their study, the group employed Multivariate Curve Resolution analysis.

In the present study, combination of PCA-LDA gave the most robust classification results. This method was also utilized by Guze et al. in a pilot study aimed at differentiating premalignant oral lesions and OSCC from physiological mucosa and benign lesions in 18 patients [27]. The authors chose classification of the acquired spectra into two groups: ≥MILD, which contained spectra from all malignant lesions and lesions with dysplasia which were histopathologically categorized as moderate or severe. And the second group as ≤LEU, which contained spectra from benign lesions, including inflammation, candidiasis or leukoplakia, and from physiological mucosa sites. Using PCA-LDA analysis, they reported the Raman spectra identified were able to discriminate between ≥MILD and ≤LEU.

In an *in vitro* study, Carvalho et al. acquired Raman spectra from cultured subcellular regions to discriminate physiological tissue from its dysplasia and OSCC [53]. From the nuclear Raman spectra, the group concluded every peak related to vibrational modes of nucleic acids could be used as a biomarker for discrimination of abnormal against normal cells. Nucleic acids were also observed to be more prominent in the spectra collected from the abnormal cell lines. The oral cavity is heterogenous, with subtle differences attributed to the presence or absence of thick, stratified, squamous, non-keratinizing mucosa in certain sites, which can be detected by Raman spectroscopy [51]. Studies using Raman and FTIR spectroscopy to detect oral premalignant diseases, indicate that anatomical site is potentially a confounding factor due to differences in the epithelium [65,66]. Sahu et al. acquired spectra from buccal mucosa, lip and tongue in healthy, contralateral (internal healthy control), premalignant and cancer conditions from 85 oral cancer and 72 healthy subjects to evaluate anatomical differences between subsites and their possible influence on healthy vs. pathological classification. The group reported major spectral differences between buccal mucosa, lip and tongue related to lipid and protein content especially

Biomedical Optics EXPRESS

in the affected and healthy, contralateral conditions. This may be because the spectrum had contribution from the stroma as well as from the epithelium [58]. In an approach to evaluate 28 healthy volunteers and 171 patients having various lesions of the oral cavity, Krishna et al. stated that subsite-anatomical differences did interfere with healthy and pathological distinction [67]. However, this may also be due to differences in experimental setup. Lastly, the cell clusters found in tumors have undergone malignant transformation and de-differentiation of their original tissue, blurring assignment to mucosal regions of the oral cavity [68]. Nevertheless, we acknowledge that the anatomical location may be a potential confounding factor. It is therefore a subject of further investigations in our group.

As emphasized previously, reduction of autofluorescence, which is inherent to viable biologic tissues, and increasing signal quality, is of high importance for subsequent data processing and statistical analysis. There are several approaches for the reduction of autofluorescence which can be divided into computation and physical methods. Computational methods use mathematical techniques, such as polynomial [69] and penalized least squares fittings [70], to approximate the autofluorescence background. Despite advancement in these techniques, they bear the risk of introducing artifacts and incapability of recognizing a Raman peak from background peaks. Physical methods for autofluorescence suppression include time-gated methods and SERDS. Time-gating takes advantage of Raman and autofluorescence processes' different interaction time to suppress the fluorescence background [71]. Even though robust and accurate, this approach requires a complicated and expensive experimental setup. A detailed comparison of these fluorescence rejection strategies with SERDS has been described by our group previously [39]. With the proposed SERDS technique, sensitivity was above 93%, underlining the potential for distinction between OSCC, non-malignant lesions and physiological mucosa [43]. Taking into account the variety of classification and experimental approaches, these data are in line with, or partly exceeding, values of the available literature where identification of oral pathologies ranged from 13 to 100% sensitivity [27,58,63–65,67]. Unique about the setup presented here, is that samples were freshly kept in their native state (isotonic 0.9% NaCl solution), without the addition of labeling agents and analyzed within a minimum time delay. Although agents such as nanoparticles may enhance spectral signal quality, their application is often not feasible in clinical routine. To our understanding, native storage *ex vivo* resembles a physiological environment of the oral cavity. While tissue fixation via formaldehyde solution is beneficial for preservation and histopathological tissue analysis, it does affect the samples' spectroscopic properties and therefore optical cancer diagnostics [72]. Moreover, the setup presented here is applicable under room light conditions, as the SERDS technique can effectively eliminate the interference of ambient light, which makes it an ideal candidate for potential application intraoperatively or in the outpatient clinic [73–75].

Although our observations indicate valid and reliable discrimination of oral lesions, limitations with this study remain. At this point in the clinical diagnostic and therapeutic pathway, there is an unmet need for immediate objective identification of an invasive OSCC against non-malignant mucosal lesions and physiological mucosa. By our SERDS-based approach, this was possible with high accuracy, although the distinction of non-malignant lesions from OSCC was more challenging than from physiological mucosa, which is plausible. There is no doubt that the group of non-malignant lesions comprises a variety of entities, with different potential for malignant transformation. Histological grading of epithelial dysplasia as mild, moderate or severe by an evaluation of cytological and architectural changes, determines potential of malignant transformation [16]. The distinction between different degrees of dysplasia, as well as detection of OPMD, is highly relevant and has vast clinical implications. Once a reliable SERDS-based method on native tissue specimens has been established as shown in this work, it may serve as the basis for distinction of subtypes and grading of oral mucosal dysplasia on a larger collective. Furthermore, the analysis was conducted *ex vivo*, under standardized conditions in the laboratory,

Biomedical Optics EXPRESS

after optimization of the experimental setup. In light of these limitations, further measurements are needed, to increase our database and lay ground for robust classification algorithms with the support of deep learning techniques. Converting the above-delineated approach into a mobile system, applicable directly in the oral cavity, with real-time measurements *in vivo*, will be a major advancement and is worthwhile being investigated.

5. Conclusion

In this work, we explored whether physiological mucosa, non-malignant lesions and oral cancer can be differentiated by Raman spectroscopy. To this end, "pure" Raman spectra of the respective tissues were isolated from heavily fluorescence interfered raw spectra using the SERDS technique. The results demonstrate that malignant and non-malignant lesions can be differentiated from physiological tissue of the oral cavity with a high accuracy, despite considerable heterogeneity of these lesions. The technique showed excellent results for the correct distinction of non-malignant lesions, that required invasive biopsy, from oral squamous cell carcinoma and physiological mucosa. The differentiation was found to be correlated to and determined by the spectral features of protein, lipid and nucleic acid.

List of abbreviations

OSCC	Oral squamous cell carcinoma
OPMD	Oral potentially malignant disorders
SERDS	Shifted-excitation Raman difference spectroscopy
PCA	Principal component analysis
LDA	Linear discriminant analysis
AUC	Area under the curve
ROC	Receiver-operating characteristic curve
FT-NIR	Fourier transformation near infrared

Funding. Wilhelm Sander-Stiftung (2017.111.1).

Acknowledgements. Werner Adler, medical informatics, biometrics and epidemiology (IMBE) at Friedrich-Alexander-Universität Erlangen-Nürnberg (FAU), provided sample size analysis and counseling for study design.

Patients' informed consent was obtained before participation. The study protocol is in accordance with the Declaration of Helsinki and has been reviewed and approved by the local Ethics Committee of the universities of Erlangen-Nürnberg (AZ 243_12 B) and Hamburg (AZ MC-309/17).

Disclosures. The authors declare that there are no conflicts of interest related to this article.

References

1. E. Omar, "Current concepts and future of noninvasive procedures for diagnosing oral squamous cell carcinoma-a systematic review," Head Face Med. **11**(1), 6 (2015).
2. F. Bray, J. Ferlay, I. Soerjomataram, R. L. Siegel, L. A. Torre, and A. Jemal, "Global cancer statistics 2018: GLOBOCAN estimates of incidence and mortality worldwide for 36 cancers in 185 countries," CA Cancer J. Clin. **68**(6), 394–424 (2018).
3. S. Warnakulasuriya, "Global epidemiology of oral and oropharyngeal cancer," Oral Oncol. **45**(4-5), 309–316 (2009).
4. C. Knipfer, J. Motz, W. Adler, K. Brunner, M. T. Gebrekidan, R. Hankel, A. Agaimy, S. Will, A. Braeuer, and F. W. Neukam, "Raman difference spectroscopy: a non-invasive method for identification of oral squamous cell carcinoma," Biomed. Opt. Express **5**(9), 3252–3265 (2014).
5. S. Marur and A. A. Forastiere, "Head and neck squamous cell carcinoma: update on epidemiology, diagnosis, and treatment," in *Mayo Clinic Proceedings*, (Elsevier, 2016), 386–396.
6. M. Mohan and N. Jagannathan, "Oral field cancerization: an update on current concepts," Oncol. Rev. **8**, 244 (2014).

Biomedical Optics EXPRESS

7. D. P. Slaughter, H. W. Southwick, and W. Smejkal, "Field cancerization in oral stratified squamous epithelium. Clinical implications of multicentric origin," Cancer **6**(5), 963–968 (1953).
8. K. Curtius, N. A. Wright, and T. A. Graham, "An evolutionary perspective on field cancerization," Nat. Rev. Cancer **18**(1), 19–32 (2018).
9. Screening, "Oral Cavity, Pharyngeal, and Laryngeal Cancer Prevention (PDQ)," in *PDQ Cancer Information Summaries [Internet]*, (Prevention Editorial Board, National Cancer Institute, Accessed: 04/29/2020, 2019), pp. https://www.cancer.gov/types/head-and-neck/hp/oral-prevention-pdq.
10. K. Wolff, F. Bootz, J. Beck, K. Bikowski, P. Böhme, W. Budach, A. Burkhardt, H. Danker, W. Eberhardt, and K. Engers, "Diagnostik und Therapie des Mundhöhlenkarzinoms," AWMF Leitlinie, 007–100 (2012).
11. S. A. Koyfman, N. Ismaila, D. Crook, A. D'Cruz, C. P. Rodriguez, D. J. Sher, D. Silbermins, E. M. Sturgis, T. T. Tsue, J. Weiss, S. S. Yom, and F. C. Holsinger, "Management of the neck in squamous cell carcinoma of the oral cavity and Oropharynx: ASCO Clinical Practice Guideline," J. Clin. Oncol. **37**(20), 1753–1774 (2019).
12. V. Grégoire, J.-L. Lefebvre, L. Licitra, and E. Felip, "Squamous cell carcinoma of the head and neck: EHNS–ESMO–ESTRO Clinical Practice Guidelines for diagnosis, treatment and follow-up," Ann. Oncol. **21**, v184–v186 (2010).
13. S. Müller, "Update from the 4th edition of the World Health Organization of head and neck tumours: tumours of the oral cavity and mobile tongue," Head and Neck Pathol **11**(1), 33–40 (2017).
14. A. K. El-Naggar, J. K. Chan, J. R. Grandis, T. Takata, and P. J. Slootweg, *WHO classification of head and neck tumours* (International Agency for Research on Cancer, 2017).
15. S. Warnakulasuriya, O. Kujan, J. M. Aguirre-Urizar, J. V. Bagan, M. A. Gonzalez-Moles, A. R. Kerr, G. Lodi, F. W. Mello, L. Monteiro, G. R. Ogden, P. Sloan, and N. W. Johnson, "Oral potentially malignant disorders: A consensus report from an international seminar on nomenclature and classification, convened by the WHO Collaborating Centre for Oral Cancer," *Oral Dis.*, https://doi.org/10.1111/odi.13704 (2020).
16. J. E. Bouquot, P. M. Speight, and P. M. Farthing, "Epithelial dysplasia of the oral mucosa-diagnostic problems and prognostic features," Curr. Diagn. Pathol. **12**(1), 11–21 (2006).
17. O. Iocca, T. P. Sollecito, F. Alawi, G. S. Weinstein, J. G. Newman, A. De Virgilio, P. Di Maio, G. Spriano, S. Pardinas Lopez, and R. M. Shanti, "Potentially malignant disorders of the oral cavity and oral dysplasia: A systematic review and meta-analysis of malignant transformation rate by subtype," Head Neck **42**(3), 539–555 (2020).
18. W. G. Shafer and C. A. Waldron, "Erythroplakia of the oral cavity," Cancer **36**(3), 1021–1028 (1975).
19. K. R. Dionne, S. Warnakulasuriya, R. B. Zain, and S. C. Cheong, "Potentially malignant disorders of the oral cavity: current practice and future directions in the clinic and laboratory," Int. J. Cancer **136**, 503–515 (2014).
20. S. Singh, O. Ibrahim, H. J. Byrne, J. W. Mikkonen, A. P. Koistinen, A. M. Kullaa, and F. M. Lyng, "Recent advances in optical diagnosis of oral cancers: Review and future perspectives," Head Neck 38, E2403-E2411 (2016).
21. K. Onizawa, N. Okamura, H. Saginoya, H. Yusa, T. Yanagawa, and H. Yoshida, "Analysis of fluorescence in oral squamous cell carcinoma," Oral Oncol. **38**(4), 343–348 (2002).
22. M. G. Müller, T. A. Valdez, I. Georgakoudi, V. Backman, C. Fuentes, S. Kabani, N. Laver, Z. Wang, C. W. Boone, and R. R. Dasari, "Spectroscopic detection and evaluation of morphologic and biochemical changes in early human oral carcinoma," Cancer **97**(7), 1681–1692 (2003).
23. A. T. Harris, A. Rennie, H. Waqar-Uddin, S. R. Wheatley, S. K. Ghosh, D. P. Martin-Hirsch, S. E. Fisher, A. S. High, J. Kirkham, and T. Upile, "Raman spectroscopy in head and neck cancer," Head Neck Oncol. **2**(1), 26 (2010).
24. A. P. Oliveira, R. A. Bitar, L. Silveira Jr., R. A. Zângaro, and A. A. Martin, "Near-infrared Raman spectroscopy for oral carcinoma diagnosis," Photomed," Photomed. Laser Surg. **24**(3), 348–353 (2006).
25. F. L. J. Cals, T. C. Bakker Schut, P. J. Caspers, R. J. Baatenburg de Jong, S. Koljenovic, and G. J. Puppels, "Raman spectroscopic analysis of the molecular composition of oral cavity squamous cell carcinoma and healthy tongue tissue," Analyst **143**(17), 4090–4102 (2018).
26. E. Barroso, R. Smits, T. Bakker Schut, I. Ten Hove, J. Hardillo, E. Wolvius, R. J. Baatenburg de Jong, S. Koljenovic, and G. Puppels, "Discrimination between oral cancer and healthy tissue based on water content determined by Raman spectroscopy," Anal. Chem. **87**(4), 2419–2426 (2015).
27. K. Guze, H. C. Pawluk, M. Short, H. Zeng, J. Lorch, C. Norris, and S. Sonis, "Pilot study: Raman spectroscopy in differentiating premalignant and malignant oral lesions from normal mucosa and benign lesions in humans," Head Neck **37**(4), 511–517 (2015).
28. H. Neumann, C. Langner, M. F. Neurath, and M. Vieth, "Confocal laser endomicroscopy for diagnosis of Barrett's esophagus," Front. Oncol. **2**, 42 (2012).
29. M. Aubreville, C. Knipfer, N. Oetter, C. Jaremenko, E. Rodner, J. Denzler, C. Bohr, H. Neumann, F. Stelzle, and A. Maier, "Automatic classification of cancerous tissue in laserendomicroscopy images of the oral cavity using deep learning," Sci. Rep. **7**(1), 11979 (2017).
30. N. Oetter, C. Knipfer, M. Rohde, C. von Wilmowsky, A. Maier, K. Brunner, W. Adler, F.-W. Neukam, H. Neumann, and F. Stelzle, "Development and validation of a classification and scoring system for the diagnosis of oral squamous cell carcinomas through confocal laser endomicroscopy," J. Transl. Med. **14**(1), 159 (2016).
31. E. J. M. Baltussen, S. G. Brouwer de Koning, J. Sanders, A. G. J. Aalbers, N. F. M. Kok, G. L. Beets, B. H. W. Hendriks, H. Sterenborg, K. F. D. Kuhlmann, and T. J. M. Ruers, "Tissue diagnosis during colorectal cancer surgery using optical sensing: an in vivo study," J. Transl. Med. **17**(1), 333 (2019).

Biomedical Optics EXPRESS

32. L. L. de Boer, T. M. Bydlon, F. van Duijnhoven, M. Vranken Peeters, C. E. Loo, G. A. O. Winter-Warnars, J. Sanders, H. Sterenborg, B. H. W. Hendriks, and T. J. M. Ruers, "Towards the use of diffuse reflectance spectroscopy for real-time in vivo detection of breast cancer during surgery," J. Transl. Med. **16**(1), 367 (2018).
33. S. Singh, H. Alam, C. Dmello, M. M. Vaidya, and C. M. Krishna, "Raman spectroscopic study of keratin 8 knockdown oral squamous cell carcinoma derived cells," in *Imaging, Manipulation, and Analysis of Biomolecules, Cells, and Tissues* (International Society for Optics and Photonics) (2012).
34. H. J. Butler, L. Ashton, B. Bird, G. Cinque, K. Curtis, J. Dorney, K. Esmonde-White, N. J. Fullwood, B. Gardner, and P. L. Martin-Hirsch, "Using Raman spectroscopy to characterize biological materials," Nat. Protoc. **11**(4), 664–687 (2016).
35. G. Chundayil Madathil, S. Iyer, K. Thankappan, G. S. Gowd, S. Nair, and M. Koyakutty, "A novel surface enhanced Raman catheter for rapid detection, classification, and grading of oral cancer," Adv. Healthcare Mater. **8**(13), 1801557 (2019).
36. A. P. Shreve, N. J. Cherepy, and R. A. Mathies, "Effective rejection of fluorescence interference in Raman spectroscopy using a shifted excitation difference technique," Appl. Spectrosc. **46**(4), 707–711 (1992).
37. K. Noack, B. Eskofier, J. Kiefer, C. Dilk, G. Bilow, M. Schirmer, R. Buchholz, and A. Leipertz, "Combined shifted-excitation Raman difference spectroscopy and support vector regression for monitoring the algal production of complex polysaccharides," Analyst **138**(19), 5639–5646 (2013).
38. J. Kiefer, "Instantaneous shifted-excitation Raman difference spectroscopy (iSERDS)," J. Raman Spectrosc. **45**(10), 980–983 (2014).
39. M. T. Gebrekidan, R. Erber, A. Hartmann, P. A. Fasching, J. Emons, M. W. Beckmann, and A. Braeuer, "Breast tumor analysis using shifted-excitation raman difference spectroscopy (SERDS)," Technol Cancer Res Treat **17**, 153303381878253 (2018).
40. M. Kasha, "Characterization of electronic transitions in complex molecules," Discuss. Faraday Soc. **9**, 14–19 (1950).
41. M. A. da Silva Martins, D. G. Ribeiro, E. A. P. dos Santos, A. A. Martin, A. Fontes, and H. da Silva Martinho, "Shifted-excitation Raman difference spectroscopy for in vitro and in vivo biological samples analysis," Biomed. Opt. Express **1**(2), 617–626 (2010).
42. S. Dochow, N. Bergner, C. Matthäus, B. B. Praveen, P. C. Ashok, M. Mazilu, C. Krafft, K. Dholakia, and J. Popp, "Etaloning, fluorescence and ambient light suppression by modulated wavelength Raman spectroscopy," Biomed. Spectrosc. Imaging **1**(4), 383–389 (2012).
43. M. T. Gebrekidan, C. Knipfer, F. Stelzle, J. Popp, S. Will, and A. Braeuer, "A shifted-excitation Raman difference spectroscopy (SERDS) evaluation strategy for the efficient isolation of Raman spectra from extreme fluorescence interference," J. Raman Spectrosc. **47**(2), 198–209 (2016).
44. J. D. Meier, D. A. Oliver, and M. A. Varvares, "Surgical margin determination in head and neck oncology: current clinical practice. The results of an International American Head and Neck Society Member Survey," Head Neck **27**(11), 952–958 (2005).
45. M. L. Hinni, A. Ferlito, M. S. Brandwein-Gensler, R. P. Takes, C. E. Silver, W. H. Westra, R. R. Seethala, J. P. Rodrigo, J. Corry, and C. R. Bradford, "Surgical margins in head and neck cancer: a contemporary review," Head Neck **35**(9), 1362–1370 (2013).
46. J. R. Maher, O. Chuchuen, M. H. Henderson, S. Kim, M. T. Rinehart, A. D. Kashuba, A. Wax, and D. F. Katz, "Co-localized confocal Raman spectroscopy and optical coherence tomography (CRS-OCT) for depth-resolved analyte detection in tissue," Biomed. Opt. Express **6**(6), 2022–2035 (2015).
47. A. Khan and H. Farooq, "Principal component analysis-linear discriminant analysis feature extractor for pattern recognition," arXiv preprint arXiv:1204.1177 (2012).
48. B. G. Tabachnick, L. S. Fidell, and J. B. Ullman, *Using Multivariate Statistics*, 5 ed. (Pearson, 2007), Vol. 5.
49. J. Bergstra, B. Komer, C. Eliasmith, D. Yamins, and D. D. Cox, "Hyperopt: a python library for model selection and hyperparameter optimization," Comput. Sci. Discovery **8**(1), 014008 (2015).
50. N. V. Chawla, K. W. Bowyer, L. O. Hall, and W. P. Kegelmeyer, "SMOTE: synthetic minority over-sampling technique," JAIR **16**, 321–357 (2002).
51. M. S. Bergholt, W. Zheng, and Z. Huang, "Characterizing variability in in vivo Raman spectroscopic properties of different anatomical sites of normal tissue in the oral cavity," J. Raman Spectrosc. **43**(2), 255–262 (2012).
52. A. C. S. Talari, Z. Movasaghi, S. Rehman, and I. U. Rehman, "Raman spectroscopy of biological tissues," Appl. Spectrosc. Rev. **50**(1), 46–111 (2015).
53. L. F. Carvalho, F. Bonnier, K. O'Callaghan, J. O'Sullivan, S. Flint, H. J. Byrne, and F. M. Lyng, "Raman micro-spectroscopy for rapid screening of oral squamous cell carcinoma," Exp. Mol. Pathol. **98**(3), 502–509 (2015).
54. F. Bonnier and H. Byrne, "Understanding the molecular information contained in principal component analysis of vibrational spectra of biological systems," Analyst **137**(2), 322–332 (2012).
55. R. Malini, K. Venkatakrishna, J. Kurien, K. M. Pai, L. Rao, V. Kartha, and C. M. Krishna, "Discrimination of normal, inflammatory, premalignant, and malignant oral tissue: a Raman spectroscopy study," Biopolymers **81**(3), 179–193 (2006).
56. C. M. Krishna, G. Sockalingum, J. Kurien, L. Rao, L. Venteo, M. Pluot, M. Manfait, and V. Kartha, "Micro-Raman spectroscopy for optical pathology of oral squamous cell carcinoma," Appl. Spectrosc. **58**(9), 1128–1135 (2004).
57. A. Mahadevan-Jansen and R. R. Richards-Kortum, "Raman spectroscopy for the detection of cancers and precancers," J. Biomed. Opt. **1**(1), 31–71 (1996).

Biomedical Optics EXPRESS

58. A. Sahu, A. Deshmukh, A. R. Hole, P. Chaturvedi, and C. M. Krishna, "In vivo subsite classification and diagnosis of oral cancers using Raman spectroscopy," J. Innovative Opt. Health Sci. **09**(05), 1650017 (2016).
59. D. V. Messadi, "Diagnostic aids for detection of oral precancerous conditions," Int. J. Oral Sci. **5**(2), 59–65 (2013).
60. R. Mehta, S. Gurudath, S. Dayansoor, A. Pai, and K. Ganapathy, "Serum lipid profile in patients with oral cancer and oral precancerous conditions," Dent. Res. J. (Isfahan **11**, 345 (2014).
61. P. Kumar, J. Augustine, A. B. Urs, S. Arora, S. Gupta, and V. R. Mohanty, "Serum lipid profile in oral cancer and leukoplakia: correlation with tobacco abuse and histological grading," J Can Res Ther **8**(3), 384 (2012).
62. S. Singh, V. Ramesh, B. Premalatha, K. V. Prashad, and K. Ramadoss, "Alterations in serum lipid profile patterns in oral cancer," J. Nat. Sci. Biol. Med. 4(2), 374 (2013).
63. B. Li, Z.-Y. Gu, K.-X. Yan, Z.-N. Wen, Z.-H. Zhao, L.-J. Li, and Y. Li, "Evaluating oral epithelial dysplasia classification system by near-infrared Raman spectroscopy," Oncotarget **8**(44), 76257–76265 (2017).
64. P.-H. Chen, R. Shimada, S. Yabumoto, H. Okajima, M. Ando, C.-T. Chang, L.-T. Lee, Y.-K. Wong, A. Chiou, and H.-O. Hamaguchi, "Automatic and objective oral cancer diagnosis by Raman spectroscopic detection of keratin with multivariate curve resolution analysis," Sci. Rep. **6**(1), 20097 (2016).
65. I. Behl, G. Calado, A. Malkin, S. Flint, S. Galvin, C. M. Healy, M. L. Pimentel, H. J. Byrne, and F. M. Lyng, "A pilot study for early detection of oral premalignant diseases using oral cytology and Raman micro-spectroscopy: Assessment of confounding factors," J. Biophotonics **13**, e202000079 (2020).
66. K. Papamarkakis, B. Bird, J. M. Schubert, M. Miljkovic, R. Wein, K. Bedrossian, N. Laver, and M. Diem, "Cytopathology by optical methods: spectral cytopathology of the oral mucosa," Lab. Invest. **90**(4), 589–598 (2010).
67. H. Krishna, S. K. Majumder, P. Chaturvedi, M. Sidramesh, and P. K. Gupta, "In vivo Raman spectroscopy for detection of oral neoplasia: a pilot clinical study," J. Biophotonics **7**(9), 690–702 (2014).
68. A. Sánchez-Danés and C. Blanpain, "Deciphering the cells of origin of squamous cell carcinomas," Nat. Rev. Cancer **18**(9), 549–561 (2018).
69. C. A. Lieber and A. Mahadevan-Jansen, "Automated method for subtraction of fluorescence from biological Raman spectra," Appl. Spectrosc. **57**(11), 1363–1367 (2003).
70. S.-J. Baek, A. Park, Y.-J. Ahn, and J. Choo, "Baseline correction using asymmetrically reweighted penalized least squares smoothing," Analyst **140**(1), 250–257 (2015).
71. T. Lipiainen, J. Pessi, P. Movahedi, J. Koivistoinen, L. Kurki, M. Tenhunen, J. Yliruusi, A. M. Juppo, J. Heikkonen, T. Pahikkala, and C. J. Strachan, "Time-gated raman spectroscopy for quantitative determination of solid-state forms of fluorescent pharmaceuticals," Anal. Chem. **90**(7), 4832–4839 (2018).
72. Z. Huang, A. McWilliams, S. Lam, J. English, D. I. McLean, H. Lui, and H. Zeng, "Effect of formalin fixation on the near-infrared Raman spectroscopy of normal and cancerous human bronchial tissues," Int J Oncol **23**, 649–655 (2003).
73. M. Maiwald, A. Müller, B. Sumpf, G. Erbert, and G. Tränkle, "Capability of shifted excitation Raman difference spectroscopy under ambient daylight," Appl. Opt. **54**(17), 5520–5524 (2015).
74. P. Vohra, P. Strobbia, H. T. Ngo, W. T. Lee, and T. Vo-Dinh, "Rapid nanophotonics assay for head and neck cancer diagnosis," Sci. Rep. **8**(1), 11410 (2018).
75. P. V. Dukes, P. Strobbia, H. T. Ngo, R. A. Odion, D. Rocke, W. T. Lee, and T. Vo-Dinh, "Plasmonic assay for amplification-free cancer biomarkers detection in clinical tissue samples," Anal. Chim. Acta **1139**, 111–118 (2020).